Renewable Energy 116 (2018) 232–243

Contents lists available at ScienceDirect

Renewable Energy

journal homepage: www.elsevier.com/locate/renene

Performance optimization of a wind turbine column for different incoming wind turbulence

V. Santhanagopalan, M.A. Rotea, G.V. Iungo*

Mechanical Engineering Department, The University of Texas at Dallas, 75080 Richardson, Texas, USA

ARTICLE INFO

Article history:
Received 1 December 2016
Received in revised form
10 May 2017
Accepted 14 May 2017
Available online 17 May 2017

Keywords:
Wind energy
Wind farm
Wind turbine
RANS
Dynamic programming

ABSTRACT

Optimization of the performance for a wind turbine column is performed by coupling a RANS solver for prediction of wind turbine wakes and dynamic programming. Downstream evolution of wind turbine wakes is simulated with low computational cost comparable to that of wake engineering models, but with improved accuracy and capability to simulate different incoming wind turbulence. Dynamic programming is used to estimate optimal tip speed ratio (*TSR*) and streamwise spacing of the turbines by using a mixed-objective performance index consisting of total power production from the entire turbine array with the penalty of the average turbulence intensity impacting over the rotor discs. The penalty coefficient, representing the economic impact of fatigue loads as ratio of wind energy revenue, is varied in order to mimic different economic periods. The results suggest that a general strategy for wind farm optimization should consist in coupling design performed through spacing optimization and using a relatively low penalty coefficient for the fatigue loads, while wind turbine operations are optimized by varying *TSR*.

1. Introduction

Maximizing performance of the already installed power plants and developing new generation tools for optimizing design and operation of wind farms continues to be an important problem [1]. Performance of a wind turbine array is determined by engineering parameters, such as wind farm layout, power curve and settings of individual wind turbines, and by the characteristics of the wind energy source, namely incoming wind velocity and turbulence. Therefore, optimization of wind farm performance is a problem involving a large number of parameters that must be simultaneously modeled and controlled.

Recent studies showed that improvements in wind power production can be achieved by switching from greedy operations of the turbines, namely operating each turbine to maximize its individual power production, to a coordinated wind turbine control to maximize power harvested from the entire wind farm [2,3]. Wind turbine controls modify not only power capture, but the produced wakes as well, thus varying the available power and added wake-generated turbulence for downstream wind turbines.

Control strategies are typically designed by means of static models for prediction of wind turbine wakes, such as wake engineering models [4,5], and rarely through more accurate large-eddy simulations (LES) due to their large computational costs [6–9]. Computational cost of the tools used for prediction of wind turbine wakes and turbine performance is crucial for wind farm design optimization (WFDO). For instance, a WFDO problem consisting of a single discretized variable of size n, such as number of turbines or number of discretized locations for turbine layout, will have a time complexity in the order of $2^n \times \beta$ for an exhaustive enumerative algorithm, where β is the time required for a single evaluation [10].

For real-time control of wind turbines and optimal design of wind farms, a good trade-off between high accuracy achievable with LES and the low computational cost of the engineering wake models is represented by solvers based on the Reynolds-Averaged Navier-Stokes (RANS) equations [11–16]. We have recently proposed a RANS solver that allows predictions of wind turbine wakes and their complex interactions within a wind farm. This RANS solver is based on a mixing length model for accurate predictions of turbulence effects on wake evolution, and parabolic approximation to drastically reduce computational costs compared to 3D global RANS solvers [17]. Furthermore, the used RANS solver allows taking into account effects of the incoming atmospheric turbulence on

* Corresponding author. Wind Fluids and Experiments (WindFluX) Laboratory, Mechanical Engineering Department, The University of Texas at Dallas, 75080 Richardson, Texas, USA.
E-mail address: valerio.iungo@utdallas.edu (G.V. Iungo).

http://dx.doi.org/10.1016/j.renene.2017.05.046
0960-1481/

Nomenclature

α	Penalty coefficient [−]
ΔP_{BL}	Percentage power difference from baseline power production [%]
δ_x	Streamwise grid spacing [m]
ν_t^{inc}	Incoming turbulent eddy-viscosity [m^2/s]
ω_{rot}	Angular rotor speed [rad/s]
$\overline{TI}$	Mean turbulence intensity at downstream turbines [−]
ρ	Density of air [kg/m^3]
a,b,c_1,c_2,c_μ	Constants [−]
C_p^{farm}	Cumulative power coefficient of wind farm [−]
C_{aero}	Aerodynamic load correction [−]
$C_{ml,i}$	Mixing length amplification factor [−]
d	Rotor diameter [m]
K	von Karman constant [−]
k	Turbulent kinetic energy [m^2/s^2]
l^*	Integral turbulent length scale [m]
l_m	Mixing length [m]
l_{wake}	Turbulent length scale [m]
N_{wt}	Number of wind turbines [−]
P	Turbine power production [$Watt$]
s_k	Normalized turbine position [−]
TI_{inc}	Incoming turbulence intensity [−]
TSR	Tip Speed Ratio [−]
U_∞	Incoming velocity [m/s]
z_{hub}	Turbine hub height [m]

wake evolution and wind turbine performance.

Optimization of wind farm design and operations can be performed with heuristic and metaheuristic methods, such as genetic algorithm, simulated annealing algorithm, pattern search algorithms, that, however, often require extensive computations, thus making them not practical for real wind farm applications. Faster solutions of WFDO problems can be attained with dynamic programming, which decomposes the optimization problem including a large number of control parameters into a sequence of subproblems with a much smaller number of control parameters [18,19]. It practically consists in optimizing sub-arrays of the initial wind farm with gradually increasing size, by adding more upstream wind turbines. For each sub-array, the objective performance index is maximized by varying parameters only for the most upstream wind turbine. Regarding the cost functional used for the WFDO problem, different models have been developed, ranging from the most widely used Mosetti's cost function [20] to more complex models [21], which consider a wider range of economic factors [22]. A technoeconomical analysis of electricity generation was performed in Ref. [23] for a location in Turkey by leveraging wind data analysis spanning a period of 36 months. In Refs. [24,25], an economic model for optimizing turbine spacing for very large wind farms was used to maximize a mixed-objective cost functional including the maximization of the power production penalized by the fatigue loads on downstream turbines.

A possible strategy to perform a coordinated wind farm control consists in varying the tip speed ratio ($TSR = \omega_{rot} d/2\, U_\infty$, where ω_{rot} is the rotor angular velocity, d is the rotor diameter and U_∞ is the freestream wind velocity) of each turbine, thus the percentage of power extracted from the available wind power. For TSR optimization, the control actuation is represented by the induction factor of the various wind turbines. Previous works showed the potential of increasing overall power production from a turbine array by derating upstream turbines in order to leave more available power for downstream wind turbines [2]. An increased power of 2.85% for a wind turbine column similar to that used in this paper has been estimated by using an empirical wake model [26]. However, larger TSR than optimal value for an isolated turbine were used, which imply higher loads on the turbines. In Ref. [26], the authors pointed out that the function of power modification consequent to derating of upstream turbines can be a non-convex function. In Ref. [27], a power increase of 1% was obtained for the Princess Amalia Wind Park. A theoretical maximum improvement was calculated to be 6%, but a more realistic estimate might yield an improvement of 3% for a spacing of 5.6 d [28].

The above-mentioned works proved the potential of increasing power production from a wind farm through a coordinated control of the wind turbines. However, to the authors' knowledge none of these works took into account the drastic variability of wind turbine performance and evolution of wind turbine wakes under different characteristics of the incoming wind velocity field and turbulence. Indeed, in this paper we will address the variability of the results achievable with a coordinated power optimization of a wind farm for different turbulence characteristics of the incoming wind. In Ref. [29], it was shown that variability of wind turbine wakes is mainly associated with the static stability of the atmospheric boundary layer. During daytime conditions, the convective stability regime leads to higher turbulence levels and lower wind shear than for nighttime stable conditions. Under convective regimes, wind turbulence facilitates flow entrainment into the wakes and faster wake recovery, thus wake interactions are less critical than for stable conditions. In Ref. [30] for an onshore wind farm, power losses were estimated to be about 4% of the total power production under stable conditions, while of only 2.4% under convective conditions.

In this paper, we carry out performance optimization for a wind turbine column by coupling an efficient RANS solver with dynamic programming. The RANS solver allows accurate estimations of the effects due to incoming wind turbulence and wake-generated turbulence on downstream evolution of wind turbine wakes. At the same time, the required computational costs are very low and comparable to those of engineering wake models, thanks to a parabolic approximation. We perform both TSR and spacing optimization for a wind turbine column in order to maximize a mixed-objective performance index consisting of the total power production from the entire turbine array with the penalty of the average turbulence intensity impacting over the rotor discs, which is considered as the main damaging factor for fatigue loads. The penalty coefficient, α, which represents the economic impact of fatigue loads on maintenance costs and durability of the wind turbines as ratio of the revenue of power production, is varied in order to mimic different economic periods. One of the main objectives of this paper is to highlight the profound effects on wind farm performance and optimal turbine settings due to different characteristics of the incoming turbulence, such as turbulence intensity and integral length scale. Furthermore, we will highlight how TSR and spacing optimization can be conveniently coupled to maximize wind farm performance.

The remainder of the paper is organized as follows: the RANS solver is described in Sect. 2. Successively, effects of incoming wind turbulence on the performance of a wind turbine column are investigated in Sect. 3. Optimization of performance for a wind

turbine column is then presented by using as control parameters both turbine *TSR* and spacing, and by considering incoming wind turbulence with different characteristics (Sect. 4). The results of the optimization study are discussed in Sect. 5. Finally, concluding remarks are reported in Sect. 6.

2. RANS solver

For this study, the CFD solver used for simulations of wakes produced by wind turbines operating with different *TSR* and different incoming turbulence is formulated through the Reynolds-averaged Navier-Stokes (RANS) equations for incompressible and axisymmetric flows [17]. The velocity and pressure fields are solved with a parabolic approximation, i.e., by advancing the RANS equations in the downstream direction and neglecting the elliptic nature of subsonic flows [31]. This strategy enables accurate predictions of flows past wind turbines with computational costs curtailed by about two orders of magnitude compared to global 3D RANS solvers [17]. This CFD tool is meant to be a valid alternative to engineering models for prediction of wind turbine wakes, such as the Jensen model [4] or the more recent Gaussian model [5], avoiding empirical tuning of model parameters and providing the capability of simulating effects of incoming turbulence and wake-generated turbulence on downstream evolution of wind turbine wakes and power production.

The RANS solver used for this study allows simulating incoming flows with different turbulence intensity, TI_{inc}, and different integral length scale, l^*, which represents the dimension of the typical large energy-containing structures present in the incoming wind. The freestream turbulent eddy-viscosity at the wind farm inlet, ν_t^{inc}, is estimated as [32,33]:

$$\nu_t^{inc} = 0.55\sqrt{\frac{3}{2}}\,\frac{TI_{inc}\,U_{\infty,1}\,l^*}{d} \tag{1}$$

Effects of different length scales of the incoming turbulence will be investigated in detail in Sect. 3, together with a variable incoming turbulence intensity.

Reynolds stresses in the RANS equations are modeled using the Boussinesq hypothesis and a mixing length model [32]. The latter provides the advantage of reproducing a volumetric variability of the turbulent eddy-viscosity and Reynolds stresses by using a parameter that is only a function of the streamwise position, namely the mixing length. For an isolated 5 MW NREL wind turbine [34], which is identical to that under examination in this paper, the mixing length was calibrated through LES data and fitted with a 4P-logistic curve [17].

LES data of a wind farm have shown that turbines operating within higher turbulence levels are characterized by larger wake Reynolds stresses, which lead to enhanced flow entrainment from the surrounding turbulent flow into the wake and a faster wake recovery [35]. This wake behavior is modeled by multiplying the calibrated mixing length for an isolated turbine by an amplification factor, $C_{ml,i}$, which is a function of the incoming turbulence. For the first turbine in the column, the amplification factor of the mixing length, $C_{ml,1}$ is of unit value for near laminar incoming condition, i.e. $TI_{inc} \leq 0.5\%$, while for higher turbulence intensity it is estimated as:

$$C_{ml,1} = \frac{c_1\,\nu_t^{inc}}{d\,U_{\infty,1}}, \tag{2}$$

where c_1 is equal to 32.8, which was calibrated based on previous LES data set of the wind turbine under examination.

Similarly, for downstream wind turbines operating within wakes generated by upstream wind turbines, the mixing length is multiplied by an amplification factor in order to take wake-generated turbulence into account. The amplification factor for the *i*th turbine, $C_{ml,i}$, is proportional to the mixing length estimated at an upstream distance of 1 d from the rotor disc using the following relation:

$$C_{ml,i} = c_2\frac{l_{m,i}}{d} + 1 \tag{3}$$

where $c_2 = 59$. The amplification factor is expected to increase downstream to each turbine due to the added wake-generated turbulence. However, to mimic the status of a fully developed wind farm after a certain number of wind turbines [36,37], which can vary for different incoming turbulence and operative conditions of the wind turbines, an upper limit to the amplification factor $C_{ml,i}$ is set to be equal to 8 [17].

The turbulent kinetic energy, k, is estimated with a parabolic approximation as follows [32]:

$$k^{n+1} = k^n + \frac{\delta_x}{U_x^n}\left[- U_r^n\frac{\partial k^n}{\partial r} - \overline{u_x u_r}^n\frac{\partial U_x^n}{\partial r} - \overline{u_\theta u_r}^n\frac{\partial U_\theta^n}{\partial r} - \frac{c_\mu^{3/4}(k^n)^{3/2}d}{l_{wake}} + \frac{\partial \nu_t^n}{\partial r}\frac{\partial k^n}{\partial r} + \frac{\nu_t^n}{r}\left(\frac{\partial k^n}{\partial r} + r\frac{\partial^2 k^n}{\partial r^2}\right)\right] \tag{4}$$

where the first term in the parenthesis represents advection of k, the second and third terms represent production, the fourth term dissipation, the fifth and sixth terms represent viscous diffusion. For turbulent dissipation, a non-dimensional length scale $l_{wake}/d = 0.32$ was calibrated based on the turbulence statistics from an LES data set. δ_x is the step for advancement of the parabolic equations in the downstream direction, c_μ is equal to 0.09 [32], while n represents a generic location in the downstream direction used for the parabolic approximation.

The wind turbine under examination is the 5 MW NREL, which has a rotor diameter of 126 m and hub height of 90 m [34]. It is noteworthy that different types of turbines can be easily simulated by providing the lift and drag coefficients for the different turbine blades. Aerodynamic forcing exerted by the turbine blades on the incoming wind is reproduced by using the actuator disc model with rotation [14,38]. The incoming wind field for each wind turbine is evaluated at an upstream distance of 1 d from the rotor disc, and it is used to estimate the local angle of attack of the turbine blade and velocity magnitude as a function of the radial position. Subsequently, lift and drag coefficients are calculated through look up tables [34]. Aerodynamic loads at tip and root of the blades are corrected through a modified Prandtl correction factor to take effects of vortices into account [39,40]. Furthermore, aerodynamic loads of the turbine are also corrected for different turbulence levels connected with upstream wind turbine wakes. This correction coefficient, $C_{aero,i}$ was calibrated separately for the thrust and tangential forces, based on an LES data set [17], as follows:

$$C_{aero,i} = a\,e^{-10(TI - TI_{inc})} + b \tag{5}$$

where a was calibrated as 0.6 and 0.21, b as 0.4 and 0.79 for the thrust and tangential forces, respectively. It is worth noticing that the aerodynamic correction is a function of the added turbulent intensity, thus it is affected by the wake-generated turbulence rather than the incoming turbulence intensity. In case TI is smaller than the incoming turbulence TI_{inc}, $C_{aero,i}$ is set to 1. The induction zone of each turbine rotor is mimicked within the parabolic framework by spreading the aerodynamic forces in the streamwise direction with a Gaussian function centered at the turbine streamwise position and with standard deviation of 0.5 d and 0.05 d

for the thrust and tangential forces, respectively. The turbine nacelle is simulated by adding a thrust force over a volume with same dimensions as for the nacelle of the 5 MW NREL turbine, namely diameter of 0.056 d and extending 0.04 d and 0.07 d upstream and downstream, respectively, to the rotor position.

At the inlet, a uniform streamwise velocity is imposed as Dirichlet boundary condition, axisymmetry conditions are imposed at the turbine axis for the three velocities in cylindrical coordinates and pressure, while at the lateral boundaries null Neumann conditions are imposed for velocities and pressure [17]. The RANS equations are discretized in the radial direction by using a Chebyshev pseudospectral collocation method implemented in Matlab. The numerical grid is mapped typically with 21 points over the rotor radius, which was determined through a previous grid sensitivity study [17]. The parabolic equations are marched in the streamwise direction by using an explicit Euler method, which is equivalent to a forward first order finite difference scheme. On a normal laptop, a simulation with a streamwise extent of about 20 d executes in less than 3 min.

The RANS solver was assessed against multiple LES cases of isolated turbines operating with different TSR and incoming turbulence intensity, as well as columns of wind turbines with different TSR and streamwise spacing [17]. For instance, Fig. 1 shows the comparison of the streamwise velocity field obtained from LES and RANS simulations for a column consisting of identical turbines, all operating in greedy conditions with $TSR = 7.5$, and a uniform streamwise spacing of 3 d. The velocity fields obtained from LES and RANS simulations, which are reported in Fig. 1a and b, respectively, result to be in very good agreement; indeed, the absolute difference between LES and RANS data is always smaller than 15% of the freestream velocity (Fig. 1c).

3. Effects of freestream turbulence on wind turbine wakes and power production

In this section, we use the RANS solver to simulate wakes associated with a column of wind turbines aligned with the wind direction, and estimate the respective power production. With this study, we aim investigating effects of the freestream wind turbulence, namely length scale, l^*, and incoming turbulent intensity, TI_{inc} (see Eq. (1)), on downstream evolution of wind turbine wakes and power production. According to the log-law similarity theory [41], a good approximation for the length scale of the freestream turbulence is $l^* = K\, z_{hub}$, where K is the von Karman constant equal to 0.41 and z_{hub} is hub height of the 5 MW NREL wind turbine, which leads to $l^*/d = 0.29$. This value is considered as upper limit for l^*; thus, for this study we have considered three values for l^*/d, namely 0.04, 0.16 and 0.29.

The baseline case consists of a column of seven turbines aligned with the wind direction, evenly spaced with a streamwise distance of 5 d and all operating in greedy conditions, i.e., with $TSR = 7.5$ that enables achieving the maximum power coefficient for an isolated wind turbine [34]. RANS simulations were performed with the three above-mentioned values of l^* and by varying TI_{inc} among 0%, 5% and 15%, which correspond to typical turbulence levels for laminar, statically stable and statically unstable boundary layer flows, respectively [30].

Fig. 2 shows streamwise velocity, tke, and turbulence intensity averaged over the rotor area, as a function of the downstream position for different values of TI_{inc} and l^*. Locations of the turbines are reported with vertical red lines. Fig. 2a shows that in proximity to the turbine locations a relatively steep reduction of the streamwise velocity is observed, which is a consequence of the power extracted by the turbines from the incoming wind, thus leading to the generation of wakes characterized by a certain velocity deficit. Moving downstream, wind velocity within the rotor area increases due to entrainment of higher momentum from the surrounding regions, thus gradually widening the wake and recovering it to the freestream incoming velocity according to the conservation of mass. The recovery rate, which is represented by the slope of the curves in Fig. 2a, varies along the turbine column and for different incoming turbulence as a consequence of the local velocity and turbulence.

It is interesting to notice that downstream to the seventh turbine, the various curves of the average velocity for the different incoming turbulence practically collapse on the same curve, which represents the condition of a fully adjusted intra-wind farm velocity field [36,37]. For further downstream turbines, the wake velocity field is mainly affected by the turbine settings and turbine spacing rather than turbulence characteristics of the incoming wind.

The evolution of the average tke within wind turbine wakes is then reported in Fig. 2b. Starting from the case with a laminar incoming flow, i.e., $TI_{inc} = 0\%$, wake turbulence increases moving downstream as a consequence of the mechanically-produced turbulence, which is connected with the velocity gradients present within the wake [32]. Moving from the first to the second turbine, a higher slope of tke is singled out due to the higher mixing length that results from an enhanced incoming turbulence generated by the first turbine. After the third turbine, the average tke starts saturating, which indicates that the mechanically-produced turbulence is practically balanced by turbulence dissipation. Indeed, downstream to the fourth turbine the variation of the tke remains

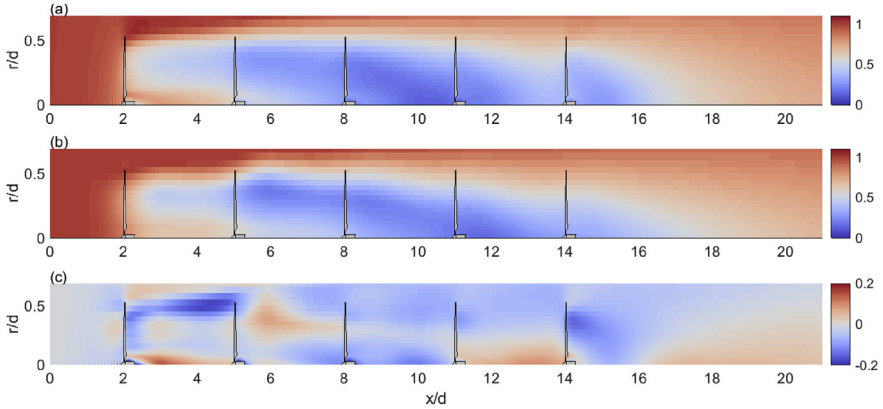

Fig. 1. Streamwise velocity for a column of wind turbines operating with a $TSR = 7.5$ and an uniform spacing of 3 d: a) LES data; b) RANS data; c) difference between LES and RANS data.

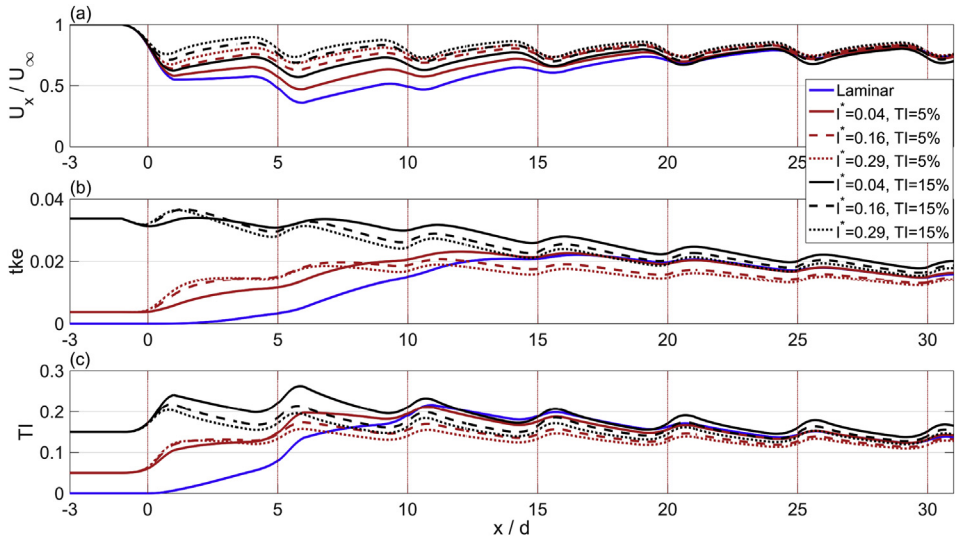

Fig. 2. Effects of incoming turbulence intensity and length scale, l^*, on wind turbine wakes: a) streamwise velocity; b) turbulent kinetic energy; c) turbulence intensity. All the parameters are estimated as average over the rotor area.

negligible.

Information gathered from the average streamwise velocity and tke can be coupled in the plot of the turbulence intensity, TI, in Fig. 2c. Downstream to the first turbine, TI increases almost linearly as a consequence of the downstream turbulence production. Downstream to the second turbine, in the near wake a higher slope of TI occurs as a consequence of the increased mixing length, but it is significantly reduced further downstream due to the faster wake recovery, i.e., increased velocity. For the following downstream turbines, the typical trend of TI is characterized by an increase in the near wake due to turbulence production of the velocity shear, followed by a decrease consequent to turbulence dissipation and wake recovery. For the laminar case, the maximum TI of 21% is detected just downstream to the third turbine, while downstream to the turbine column, it is equal to only 13%.

Increasing TI_{inc} to 5% and 15%, the average tke increases faster in the near wake as a consequence of the enhanced mixing length according to Eq. (3). Fig. 2b shows that for the cases with TI_{inc} equal to 5% and 15%, the competition between turbulence production and dissipation already occurs downstream to the first turbine. For the case with $TI_{inc} = 15\%$, a gradual reduction of the average tke over the rotor area is observed by moving downstream, which leads to TI = 14%, which is very close to the value obtained for a laminar incoming flow. The main parameter in the RANS solver controlling the budget between mechanically turbulence production and turbulence dissipation is the length scale for wake-generated turbulence, l_{wake} (Eq. (4)).

As expected, effects of an increased l^* are similar to those of an increased turbulence intensity. This analysis enforces the synergistic role of turbulence intensity and integral length scale of the freestream turbulence for the flow field within a wind farm.

The condition of a fully developed intra-wind farm wind field is achieved at slightly shorter downstream distances for higher incoming turbulence and larger l^*. This may suggest that for a fully adjusted intra-wind farm flow, wake-generated turbulence might be more significant than incoming freestream turbulence. On the other hand, incoming turbulence is highly important for the wake velocity field of the first turbine rows and for the downstream distance where the intra-wind farm flow achieves a fully adjusted condition.

The normalized power production from each turbine for the baseline case and different incoming turbulence characteristics is shown in Fig. 3. The plot for laminar incoming condition shows a good agreement with the corresponding LES case consisting of 3 turbines in the column, while the other plots indicate the effect of the turbulence length scale and different turbulence intensity. As expected, increases in both TI_{inc} and l^* lead to higher power production of the downstream turbines, especially for the first few turbine rows. Furthermore, we also notice the turbine column reaches a fully developed wind farm condition, here characterized by a roughly invariant power production, faster as we increase either the incoming turbulence or the length scale. In practice, the different cases reported in Fig. 3 are piled as a function of the incoming turbulent eddy viscosity, ν_t^{inc}, moving from zero for the laminar case to the maximum value for $TI_{inc} = 15\%$ and $l^*/d = 0.29$.

For the case with a laminar incoming flow, the turbine with the minimum power production is turbine 3, which has a power production of only about 10% of an isolated turbine operating with TSR = 7.5. The second turbine follows with a power production of 16.3%, while moving downstream the power production starts increasing. From the RANS simulations performed for different turbulence characteristics of the incoming wind, it is evident that the largest power losses generally occur at the turbine 2 or 3.

4. Performance optimization performed with dynamic programming

The RANS solver has been developed in order to provide a compelling tool for accurate predictions of wind turbine wakes with a low computational cost. Therefore, it is suitable for optimization of wind farm operations for which a large number of wake predictions is needed to achieve convergence of the optimization process. In this section, optimization will be performed for a turbine column consisting of 5 turbines deployed over a land with fixed streamwise extent of 20 d, different atmospheric conditions, and using two control variables, namely *TSR* and turbine position. Fig. 4 shows the schematic of the optimization problem.

An economic model is considered for the optimization of wind farm performance. Since, the number of turbines and land size is fixed, their respective costs are constant and, thus, not included in the optimization problem. According to previous works [25,42,43], we assume the turbulence intensity over the rotor disc as main damaging factor for fatigue loads. The influence on the fatigue loads of different wind parameters, such as mean wind speed, turbulence

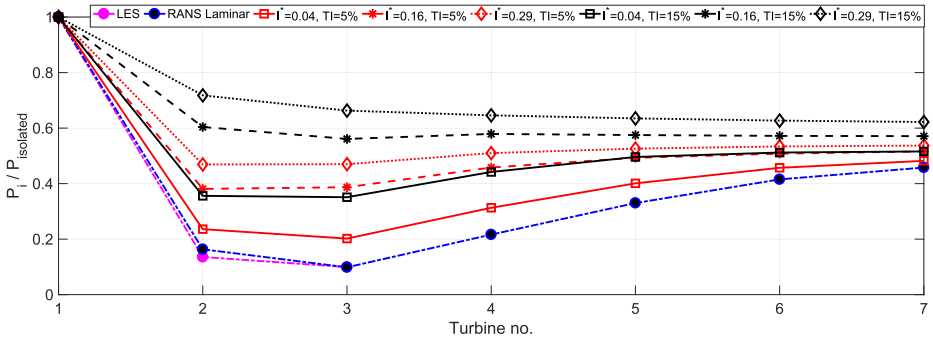

Fig. 3. Effects of turbulence length scale, l^*, and incoming wind turbulence intensity, TI_{inc}, on power production for seven turbines evenly spaced with a distance of 5 d and all operating at $TSR = 7.5$.

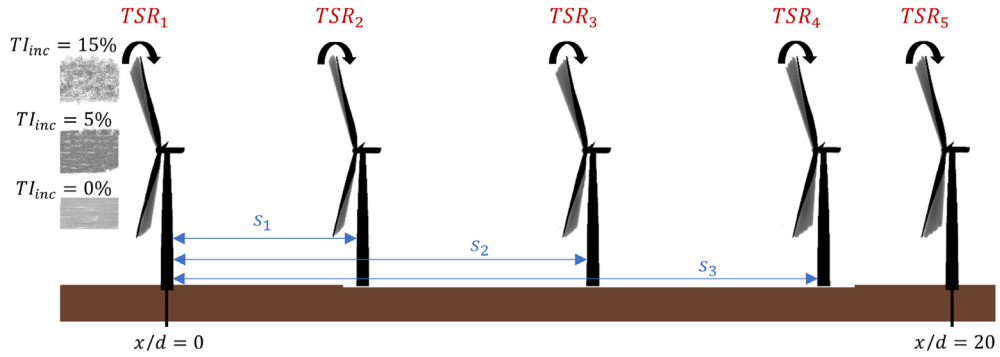

Fig. 4. Schematic of the optimization problem showing different incoming wind turbulence intensities, TSR_i and position, s_i, for each turbine.

intensity, length scales, vertical shear of velocity, yaw misalignment, was shown in Ref. [43]. Indeed, it was found that the fatigue loads in blade flapwise bending moment are primarily affected by turbulence intensity, and increased up to 60% for a 10% increase in turbulence intensity, for a turbine operating in flat terrain. Therefore, the mixed-objective performance index for the optimization problem is formulated as:

$$J = \frac{\sum_{j=1}^{N_{wt}} P_j}{\frac{1}{2}\rho\pi\frac{d^2}{4}U_{\infty,1}^3} - \alpha \sum_{j=2}^{N_{wt}} TI_j \tag{6}$$

where N_{wt} is the total number of wind turbines in the column, ρ is air density, d is the rotor diameter, P_j and TI_j are power production and turbulence intensity averaged over the rotor disc, respectively, for the j-th turbine. The first term on the right-hand-side represents the power production from the entire turbine column made non-dimensional through the incoming freestream wind velocity, $U_{\infty,1}$, while the second term is the penalty due to the fatigue loads and α is the respective penalty coefficient. It is noteworthy that the average turbulence intensity over the most upstream turbine, TI_1, is not included in the penalty being only a function of the incoming turbulence intensity. The penalty coefficient can vary significantly according to time and location of the wind farm, as the market value of wind power varies [44,45]. In this work, the following values are considered $\alpha = 0, 0.05, 0.5, 2$. The case $\alpha = 0$ is equivalent to only power maximization, while higher α-values increase weight given to the maintenance costs due to effects of fatigue loads on turbine durability or represent a lower economic profitability of wind power production.

4.1. TSR optimization for an evenly-spaced turbine column

The problem of finding the optimal *TSR* values for a turbine column is solved through dynamic programming [18,19,46]. The theoretical justification for using dynamic programming for wind farm power maximization was provided in Refs. [18,19]. In Ref. [18], a dynamic programming algorithm using an analytical actuator disc model was proposed, while it was studied in Ref. [19] using a near-wake and far-wake model, both developed using engineering wake models. These authors also suggested the applicability of dynamic programming by leveraging high fidelity models. While [47] used a high-fidelity LES code for verifying the results, the dynamic programming optimization was still performed using the Jensen wake model. In this work, the RANS solver introduced in Sect. 2 is used with the dynamic programming algorithm derived in Ref. [18]. Considering wind advection in the positive streamwise direction, the control performed on the last turbine does not affect the upstream turbines. Hence a multistage recursive optimization process is used in dynamic programming with a backward induction, i.e. starting from the last turbine. Specifically, for *TSR* optimization of a column of five turbines, we generate five sub-problems starting from the most downstream turbine and gradually adding one upstream turbine. For each sub-problem, *TSR* is only optimized for the most upstream turbine, while downstream turbines are set with their optimal *TSR* determined through the previous optimization steps [18]. For the *TSR* optimization, the mixed-objective performance index in Eq. (6) can be written for the i-th dynamic programming step as:

$$J(TSR_{N_{wt}-i+1}) = \frac{1}{\frac{1}{2}\rho\pi\frac{d^2}{4}U_{\infty,N_{wt}-i+1}^3}\sum_{j=1}^{i} P_{N_{wt}-j+1} - \alpha\sum_{j=2}^{i} TI_{N_{wt}-j+2} \tag{7}$$

4.2. Spacing optimization

Considering a heterogeneous turbine spacing leads to a new optimization parameter, namely the position variable, s_k, which is

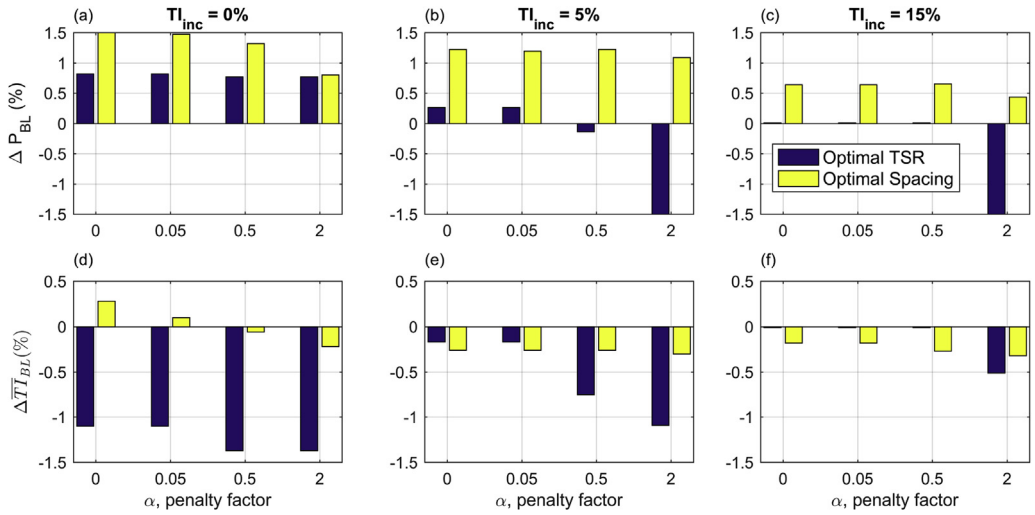

Fig. 5. TSR and spacing optimization by varying the penalty coefficient α: a, b, c) Percentage difference of cumulative power; d, e, f) Difference in mean turbulence intensity, $\overline{TI}$. The three columns are for incoming turbulence intensity, TI_{inc}, of: a, d) 0%; b, e) 5%; c, f) 15%.

defined as the distance of the turbine k from the most upstream turbine. With the constraints of a fixed land area, i.e. fixed distance between the first and the last turbine in the column, and a fixed number of turbines $N_{wt} = 5$, optimization is then performed by varying s_k with k = 2, 3, 4 and maximizing the mixed performance index in Eq. (6).

For the $k-th$ turbine, an increased distance from the most upstream turbine results in a larger distance for enhanced wake recovery and, in turn, higher wind velocity and lower wake-generated turbulence intensity occurring over the rotor of the considered turbine. However, an increase of the position s_k leads to a smaller separation distance from the next downstream turbine, thus less available power and enhanced fatigue loads for the downstream turbine. Therefore, it is easily explained the need for solving an optimization problem, thus finding a trade-off among the available power and turbulence intensity for the various turbines.

While existing works on dynamic programming for power optimization of wind farms were performed using as control variable the induction factor or the *TSR*, the dynamic programming algorithm developed in Ref. [18] can also be used with other optimization variables, such as the turbine position. Indeed, the principle of optimality, upon which the dynamic programming was applied for a column of wind turbines, remains unaltered by using a different control variable. Following dynamic programming [18], we begin simulating the baseline case of five turbines set with $TSR = 7.5$, uniform spacing of 5 d, then performing spacing optimization from the turbine $k = N_{wt}-1$ to $k = 2$, and varying only s_k at each optimization step. The minimum distance between two consecutive turbines is constrained to 2 d, while increments in s_k are multiples of 0.25 d.

5. Results of performance optimization

The results of the optimization problem defined in Sects. 4.1 and 4.2 are shown in Fig. 5, where the first row represents the percentage difference in power production between the optimal and the baseline configuration, which consists of the same incoming turbulence intensity, all the turbines evenly spaced with a distance of 5 d and under greedy operation at $TSR = 7.5$. The second row represents the difference in mean turbulence intensity experienced by the downstream turbines of the column ($\overline{TI} = \sum_{j=2}^{N_{wt}} TI_j/(N_{wt}-1)$). In Fig. 5, the three columns correspond to incoming turbulence intensities $TI_{inc} = 0\%$, 5% and 15%. The blue-colored bars in the plots show the results from only *TSR* optimization (Sect. 4.1), while the yellow-colored bars show results from

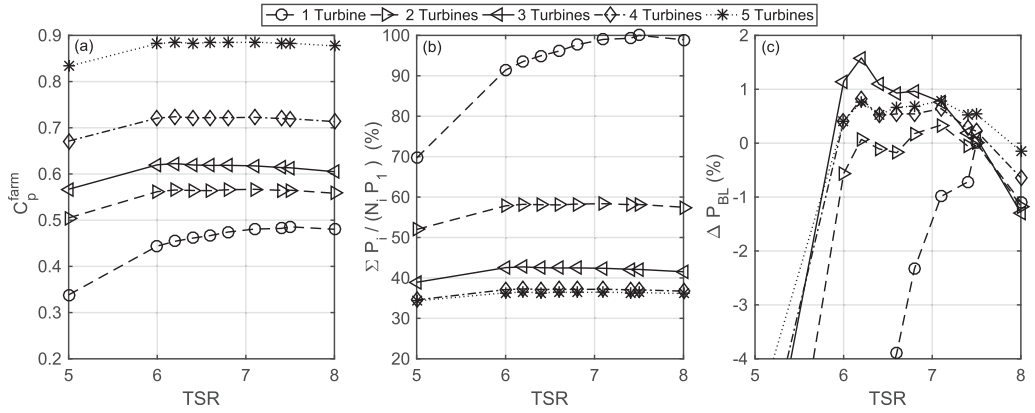

Fig. 6. Power maximization with *TSR* optimization of a column with five turbines, streamwise spacing of 5 d and laminar incoming wind: a) cumulative power coefficient of the wind farm; b) efficiency of the wind farm; c) percentage difference between cumulative power of the turbine sub-array and the baseline case.

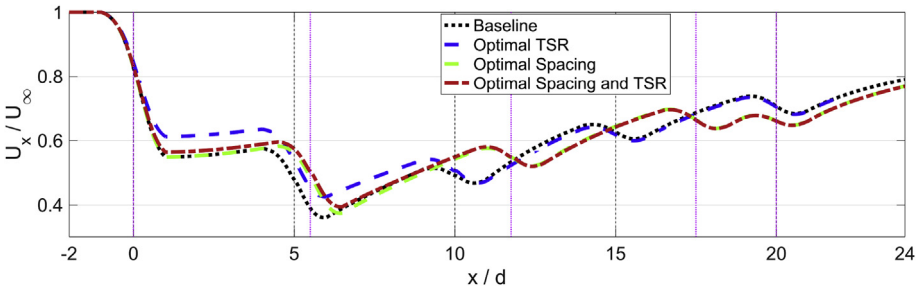

Fig. 7. Comparison of the streamwise velocity averaged over the rotor area for the baseline case, *TSR*-optimized configuration, optimally-spaced configuration all the turbines set with $TSR = 7.5$, and configuration optimized in spacing and *TSR* by considering laminar incoming flow ($TI_{inc} = 0\%$) and power maximization ($\alpha = 0$).

performing only spacing optimization (Sect. 4.2). In each figure, the various bars represent results by using four different values of the penalty coefficient, α, namely 0, 0.05, 0.5 and 2.

5.1. Maximization of power production

By considering a null penalty coefficient in Eq. (6) ($\alpha = 0$), the optimization problem reduces to the power maximization for the entire turbine column. From Fig. 5a–c, it is observed that spacing optimization generally produces larger power increments than performing *TSR* optimization. It is interesting to note from Fig. 5d–f that even performing only power optimization with $\alpha = 0$, the optimal configuration always leads to reduction of fatigue loads, except for the spacing optimization for an incoming turbulence intensity of $TI_{inc} = 0\%$. These results suggest that increase (decrease) of the distance from the upstream turbine or a reduction (increase) of *TSR* of the upstream turbine lead to higher (lower) wind velocity, thus available power, and lower (higher) wake-generated turbulence, thus fatigue loads. Furthermore, the TSR optimization while producing lesser power improvement than spacing optimization, results in a greater reduction of the average turbulence intensity, $\overline{TI}$.

Fig. 6 shows the results for the *TSR* optimization for the case of power maximization ($\alpha = 0$) and laminar incoming wind ($TI_{inc} = 0\%$). The different subplots of Fig. 6 depict the same results of the *TSR* optimization from different perspectives. Fig. 6a shows the overall power production for each stage of the dynamic programming optimization process in terms of cumulative power coefficient of the wind farm. At the first step, power is optimized only for the most downstream wind turbine, i.e., turbine 5. Variation of the *TSR* produces a power curve analogous to that of the 5 MW NREL wind turbine [34]. Following the Bellman's principle of optimality [18,46], we expect the most downstream turbine to operate at *TSR* corresponding to the maximum power production for an isolated turbine, i.e. $TSR = 7.5$. Indeed, the wake associated with the most downstream turbine does not produce any detrimental effect on the remaining upstream turbines.

At the second step of the dynamic programming optimization, the sub-array consisting of turbines 4 and 5 is considered. As shown in Fig. 6a, the parameter $C_{p,2}^{farm}$ is estimated by varying *TSR* of the turbine 4, while *TSR* of turbine 5 remains fixed at its optimal value of 7.5. The optimal $C_{p,2}^{farm}$ is obtained at $TSR = 7.1$ for the turbine 4. Proceeding with the dynamic programming optimization up to the most upstream turbine, namely turbine 1, the optimal configuration for a laminar incoming flow is estimated to be with *TSR* equal to 6.2 - 6.2 - 6.2 - 7.1 - 7.5, moving from the most upstream turbine towards downstream. This optimal configuration enables power increase of 0.8% over the baseline case.

Fig. 6a shows a monotonic increase of $C_{p,i}^{farm}$ by adding more upstream wind turbines to the turbine column. However, this might be a misleading information derived by the larger power extracted from the incoming wind power, which is merely a consequence of a larger number of turbines included in the array. Therefore, it can be convenient to analyze performance of a wind turbine column through efficiency of the turbine array, $(\Sigma P_i)/(N_i P_1)$, which is defined as ratio between the cumulative power production from the array and the potential power extracted by the same number of turbines operating under isolated conditions. Fig. 6b shows that efficiency of the wind farm gradually decreases by adding more turbines to the array, which is clearly connected with the wake losses produced by upstream wind turbines. Furthermore, from both Fig. 6a and b it is observed that increasing the number of turbines, the cumulative power curves become flatter within the range $6 \leq TSR \leq 8$, which indicates a limited potential of increasing power production by optimizing *TSR* of the wind turbines.

This feature can better be highlighted by plotting the difference between the power production from the optimized array and the baseline case as percentage of the power production from the baseline case. Fig. 6c shows that for the step 2 of the dynamic programming optimization, namely considering a sub-array of only two turbines, the potential of increasing power production with respect to the baseline case is practically negligible. Conversely, at the step 3 for an array of three turbines, the maximum potential for power optimization is estimated. Indeed, by setting the turbines with *TSR* 6.2 - 7.1 - 7.5, moving downstream from the most upstream turbine, a power increase of 1.6% is achieved with respect to the baseline case. This result is in agreement with the analysis of the wind farm velocity field presented in Fig. 2 and the consequent power production reported in Fig. 3. The second and the third turbines are typically characterized by the largest power losses due to wake interactions, thus these turbines can largely benefit from derating the most upstream turbine.

With a larger number of turbines, the cumulative power curves become flatter, indicating that *TSR* of more upstream turbines do not affect significantly the slope of the overall power curve of the turbine column and the typical power improvement is about 0.8% over the baseline case. This is in agreement with the results obtained for a similar study performed with LES and the Jensen model [47]. However, in that work a stronger derating of upstream turbines was performed, which might be a consequence of the tuning of the wake expansion parameter for the Jensen model [4].

To gain a physical understanding of the results obtained from the different optimization processes to perform power maximization ($\alpha = 0$) for the case of laminar incoming wind ($TI_{inc} = 0\%$), the streamwise velocity averaged over the rotor area is reported in Fig. 7 and power production from individual turbines is reported in Fig. 8. In both figures, the baseline case, the *TSR*-optimized configuration, the optimally-spaced configuration with all turbines operating with $TSR = 7.5$, and the configuration optimized first in spacing and then in *TSR* are reported. In Fig. 7, the streamwise positions of the turbines for the case with uniform spacing are reported with vertical black dashed lines, while those for the space-optimized configurations are reported with vertical pink lines.

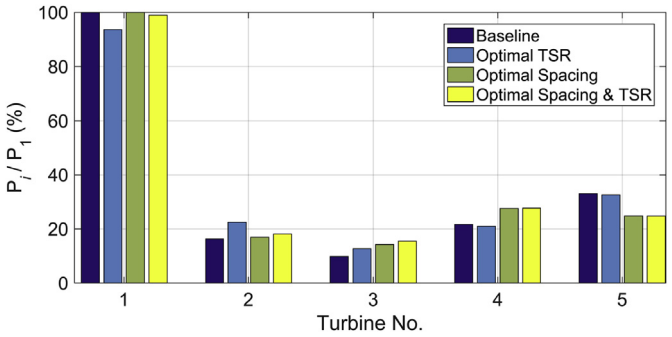

Fig. 8. Power maximization ($\alpha = 0$) by considering laminar incoming flow. Power production of individual turbines as percentage of the power from an isolated turbine with $TSR = 7.5$ for the different optimized configurations.

Starting from the *TSR* optimization and all the turbines evenly spaced with a distance of 5 *d*, Fig. 8 shows that derating turbine 1 with $TSR = 6.2$ leads to a curtailed power production of about 94% with respect to the greedy condition. Concurrently, a higher velocity is produced in the wake of the derated turbine 1, which leads to higher power for the turbines 2 and 3 (respective power increase of 6% and 3% over the baseline case). Effects of *TSR* optimization become practically negligible for the remaining downstream wind turbines. This confirms that *TSR* optimization is primarily advantageous for turbines 2 and 3, which are the turbine mostly affected by wake-generated power losses.

For the spacing optimization, there is an increase in the incoming velocity for turbines 2, 3 and 4, as compared to the baseline case with uniform spacing, which is a consequence of the larger streamwise spacing and, in turn, to the extended wake recovery leading to higher available power for downstream wind turbines. However, incoming velocity is slightly reduced for turbine 5 due to the short spacing of 2.5 *d* from the adjacent upstream turbine, which is a consequence of the constrained land area.

Finally, *TSR* optimization performed on the space-optimized column leads to a further increase in power production by about 0.8%, which is, as expected, due to the derating of the most upstream turbine and slight improvements for the downstream turbines. It is interesting to note that this optimized *TSR* configuration 7.1 - 7.1 - 6.2 - 7.1 - 7.5, has a slightly higher *TSR* for the upstream turbines as compared to the respective optimized *TSR* configuration for a uniformly spaced array. This again is a consequence of the increased spacing for the upstream turbines.

A detailed summary of the results of the optimization problem performed for $\alpha = 0$, thus maximizing power production, is presented in Table 1. For laminar incoming wind, spacing optimization leads to a power increase of 1.5% with the configuration of s_k equal to 5.5 *d* - 11.75 *d* - 17.5 *d*, for turbine 2, turbine 3 and turbine 4, respectively. If the baseline case is *TSR*-optimized, then a power increase of 0.8% is achieved. Indeed, spacing optimization always produces higher power increase than *TSR* optimization. Therefore, a suitable strategy may consist in performing first spacing optimization, then the space-optimized configuration is further improved by varying *TSR* from greedy conditions. Indeed, coupling spacing and *TSR* optimization allows achieving power increase of 2.2%.

By increasing the incoming turbulence intensity to 5% and 15%, the power production of the baseline case increases of 50.4% and 83.5%, respectively. Therefore, room for power improvements is reduced for higher incoming turbulence intensity, which is mainly due to the faster wake recovery and, in turn, reduced wake interactions. It can be seen from the results of optimal *TSR* configuration in Table 1, that the upstream turbines are weakly derated as the freestream turbulence intensity is increased. Indeed, for $TI_{inc} = 15\%$ the optimal *TSR* configuration is the same as the baseline case, implying that the power cannot be increased significantly by performing only *TSR* optimization. Similarly, when comparing the optimal layout obtained through spacing optimization for the three incoming turbulence cases, it is seen that the spacing between the last two turbines in the optimal configuration increases as the turbulence intensity is increased, while still being lower than the baseline spacing of 5 *d*. In general, it is seen that the intermediate turbines in the optimally spaced configuration have a larger s_k than the uniformly spaced baseline case. Similar, to the *TSR* optimization, the optimally spaced configuration was closer to the baseline configuration, as the TI_{inc} was increased. By coupling *TSR* and spacing optimization power increase of 1.3% and 0.6% are attained for incoming turbulence intensity of 5% and 15%, respectively, which are mainly achieved with the spacing optimization.

These results reflect effects of the incoming wind turbulence on downstream evolution of wind turbine wakes and, in turn, on power production. By increasing the incoming wind turbulence, a faster wake recovery occurs leading to higher available wind power for downstream wind turbines [17,29,30]. Therefore, for a given wind farm layout, derating upstream turbines, which leads to a reduction of the power production of the derated turbines, turns out to be a positive effect only if it entails higher available power for downstream turbines. In case a sufficient wake recovery already occurs, which is a combination of wind turbine settings, downstream distance among turbines and freestream turbulence, then derating upstream turbines may turn out to be a detrimental control action.

5.2. Maximization of the mixed-objective performance index

In scenarios where the importance of decreasing fatigue loads is higher or when the electricity demand or load of the wind farm is less, the value of the penalty coefficient, α, in the mixed-objective performance index in Eqs. (6) and (7) is increased to improve the life and durability of the turbines. Reviewing once again Fig. 5, the results on power production and $\overline{TI}$ for $\alpha = 0.05$, 0.5 and 2, are then discussed.

Performing only *TSR* optimization, the optimal configuration for the various incoming wind conditions, does not change for the penalty coefficient $\alpha = 0.05$ from power maximization with $\alpha = 0$. Increasing α to 0.5, for laminar incoming condition, the *TSR* optimization reduces $\overline{TI}$ by 0.27% without significant compromise in power production. The *TSR* optimization for $TI_{inc} = 5\%$, helped significantly reduce $\overline{TI}$ by a value of 0.58%, while also decreasing the power production to a lower value than that for the baseline case. However, for higher incoming turbulence $TI_{inc} = 15\%$, the resulting configuration was the same as for $\alpha = 0.05$, namely the baseline configuration. The *TSR* optimization with highest penalization factor $\alpha = 2$ for $TI_{inc} = 0\%$, results in the same configuration as for $\alpha = 0.5$. For the cases with higher incoming turbulence $TI_{inc} = 5\%$ and 15%, using the highest penalization weight of $\alpha = 2$ in *TSR* optimization, leads to a drastic reduction in power while reducing $\overline{TI}$ by a maximum of 0.5%.

For stable and convective incoming conditions ($TI_{inc} = 5\%$ and 15% respectively), spacing optimization with $\alpha = 0.05$ produces the same configuration as for $\alpha = 0$. However, for the laminar incoming condition, $TI_{inc} = 0\%$, this penalization factor results in a $\overline{TI}$ reduction of 0.2% without any noticeable compromise in power production. For $\alpha = 0.5$ the spacing optimization leads to a reduction of 0.2% on both power and $\overline{TI}$ for laminar incoming wind, while negligible variations are observed for $TI_{inc} = 5\%$ and 15%. Finally, the layout-optimization with highest penalization factor $\alpha = 2$ for $TI_{inc} = 0\%$, helps reducing the $\overline{TI}$ by 0.2%, but affecting power production significantly. Similarly, for higher incoming turbulence of $TI_{inc} = 5\%$ and 15%, negligible reduction in fatigue loads is achieved

Table 1
Percentage power increment for the various optimized configurations with respect to the baseline case with laminar flow, ΔP_{BL0}, and baseline case with same incoming turbulence intensity, ΔP_{BL}, and difference of average turbulence intensity at downstream turbines, $\overline{TI}$, between optimal configurations and respective baseline case.

Case	Configuration		TI_{inc}%	ΔP_{BL0}	ΔP_{BL}	$\overline{TI} - \overline{TI}_{BL}$
Baseline 0%	Position TSR	5-10-15 7.5-7.5-7.5-7.5-7.5	0	0.0%	0%	0%
Spacing Opt. 0%	Position TSR	5.5-11.75-17.5 7.5-7.5-7.5-7.5-7.5	0	1.5%	1.5%	0.28%
TSR Opt. 0%	Position TSR	5-10-15 6.2-6.2-6.2-7.1-7.5	0	0.8%	0.8%	−1.10%
Spacing-TSR Opt. 0%	Position TSR	5.5-11.75-17.5 7.1-7.1-6.2-7.1-7.5	0	2.2%	2.2%	0.04%
Baseline 5%	Position TSR	5-10-15 7.5-7.5-7.5-7.5-7.5	5	50.4%	0%	0%
Spacing Opt. 5%	Position TSR	6-12.5-17 7.5-7.5-7.5-7.5-7.5	5	52.2%	1.2%	−0.26%
TSR Opt. 5%	Position TSR	5-10-15 7.1-7.1-7.1-7.1-7.5	5	50.8%	0.3%	−0.17%
Spacing-TSR Opt. 5%	Position TSR	6-12.5-17 7.1-7.1-7.1-7.1-7.5	5	52.3%	1.3%	−0.41%
Baseline 15%	Position TSR	5-10-15 7.5-7.5-7.5-7.5-7.5	15	83.5%	0%	0%
Spacing Opt. 15%	Position TSR	5-11-16 7.5-7.5-7.5-7.5-7.5	15	84.6%	0.6%	−0.18%
TSR Opt. 15%	Position TSR	5-10-15 7.5-7.5-7.5-7.5-7.5	15	83.5%	0%	0%
Spacing-TSR Opt. 15%	Position TSR	5-11-16 7.5-7.5-7.5-7.5-7.5	15	84.6%	0.6%	−0.18%

Table 2
Percentage power increment and $\overline{TI}$ difference with respect to the baseline case with $TI_{inc} = 5\%$, for the economic model TSR-optimization of the optimized layout for various values of the penalty coefficient α.

α	Case	Configuration		TI_{inc}%	ΔP_{BL}	$\overline{TI} - \overline{TI}_{BL}$
0	Spacing Opt.	TSR Position	7.5-7.5-7.5-7.5-7.5 6-12.5-17	5	1.2%	−0.26%
0	TSR-Opt. for optimized spacing	TSR	7.1-7.1-7.1-7.1-7.5	5	1.3%	−0.41%
0.4	TSR-Opt. for optimized spacing	TSR	7.1-7.1-7.1-6.2-7.5	5	0.9%	−0.50%
0.45	TSR-Opt. for optimized spacing	TSR	7.1-7.1-6.2-6.2-7.5	5	0.4%	−0.57%
0.5	TSR-Opt. for optimized spacing	TSR	6.2-7.1-6.2-6.2-7.5	5	−0.2%	−0.99%

with a noticeable power reduction.

This economic analysis confirms that *TSR* optimization is more beneficial for decreasing fatigue loads while spacing optimization allows achieving better performance in power production. It is evident that a penalty for fatigue loads in the optimization problem with $\alpha = 2$ leads to drastic reduction in power, while $\alpha = 0.05$ produces similar results as for the case with $\alpha = 0$. The penalty factor $\alpha = 0.5$ was found to be a good trade-off in reducing the fatigue loads without compromising noticeably power production.

According to these results, it is deemed convenient to perform spacing optimization for maximizing power production. Subsequently, with the resulting optimized layout, *TSR* optimization can be performed with an economic model for α around 0.5, to reduce the fatigue loads without compromising significantly on the power production. For the case with incoming wind turbulence $TI_{inc} = 5\%$, spacing optimization for maximizing power produces optimal positions 6-12.5-17 for the three intermediate turbines, which are then optimized for *TSR* with $\alpha = 0.4$,0.45 and 0.5. The results presented in Table 2 shows the sensitivity to α of the optimized configuration, power production and added fatigue loads.

6. Conclusions

Optimization of the performance for a wind turbine column has been performed by coupling a newly-developed RANS solver and dynamic programming. Predictions of wakes and power production of wind turbines operating with different values of the tip speed ratio, *TSR*, and incoming wind turbulence have been carried out with the proposed RANS solver, for which turbulence closure is carried out with a mixing length model. Parabolic and boundary layer approximations in the RANS solver allows achieving very low computational costs comparable to those of engineering wake models and improved accuracy. However, accuracy in prediction of the turbulent kinetic energy might be affected by the above mentioned approximations and estimations of the turbulent length scales of the incoming and wake-generated turbulence.

Optimization on *TSR* of the wind turbines has shown that a maximum power improvement of 0.8% is achievable for a column of five wind turbines evenly spaced with a distance of 5 d and laminar incoming wind field, while also decreasing the average turbulence intensity experienced by the downstream turbines by 1.1%. The power increase is achieved by derating the upstream wind turbine allowing enhanced residual wind power for downstream wind turbines and reducing shear generated turbulence. However, *TSR* optimization is practically ineffective to increase power production for highly turbulent incoming wind fields. Indeed, in presence of wind turbulence, enhanced mixing and flow entrainment lead to a faster wake recovery and reduced effects of

detrimental wake interactions. Thus, derating upstream wind turbines does not affect significantly the available power for downstream turbines in presence of a turbulent incoming wind. On the other hand, derating of the upstream turbines helps reducing the fatigue loads throughout the turbine column up to 1%, while also entailing power reduction from the entire turbine column. Based on economic considerations, a suitable compromise between power increment and fatigue load reduction should be achieved according to different incoming wind turbulence.

The RANS solver has also been used in combination with dynamic programming to perform spacing optimization of a wind turbine column with the constraints of a fixed land area and total number of turbines. It has been shown that a turbine column optimized only in spacing, yields higher power improvement than performing only *TSR* optimization. A combination of spacing and *TSR* optimization, and operating with a laminar incoming wind, allows producing 2.2% more power than the baseline case with evenly spaced turbines operating in greedy conditions. A holistic approach towards maximizing profit over the lifetime of the wind farm, suggests that spacing optimization in maximizing power production be performed initially, followed by performing real-time *TSR* optimization for an economic model considering power production and maintenance costs associated with fatigue loads.

This study has highlighted that results of the various optimization processes are highly sensitive to the incoming wind turbulence and wake-generated turbulence, and thus the importance of the daily cycle of atmospheric stability in design and operation of wind farms. Indeed, by considering an incoming turbulence intensity of 15%, a power variation as high as 83% over the baseline case with laminar incoming wind has been documented, while, in contrast, power improvements obtained through model-based optimization are typically smaller than 10%. Therefore, it is very important to perform optimization of wind farm operations using models or CFD tools that enable accurate predictions of the interactions between a turbulent wind field and a wind turbine array. In future, robust fault detection techniques and fault tolerant control approach introduced for wind turbine applications [48,49], can be performed by coupling the power predictions obtained through the RANS solver and SCADA data. Furthermore, we suggest performing a synergistic design of wind farm layout and control strategies according to the specific characteristics of the wind field over the test site under examination.

Acknowledgments

This work was partially funded by the National Science Foundation under the I/UCRC WindSTAR, NSF Award IIP 1362033.

References

[1] S. Lindenberg, B. Smith, K. O'Dell, 20% Wind Energy by 2030, Tech. rep., National Renewable Energy Laboratory (NREL), US Department of Energy, Renewable Energy Consulting Services, Energetics incorporated, 2008.
[2] T. Knudsen, T. Bak, M. Svenstrup, Survey of wind farm control-power and fatigue optimization, Wind Energy 18 (2015) 1333–1351.
[3] G.V. Iungo, F. Viola, U. Ciri, S. Leonardi, M. Rotea, Reduced order model for optimization of power production from a wind farm, in: 34th Wind Energy Symposium, 2016, p. 2200.
[4] N. Jensen, A Note on Wind Turbine Interaction, Tech. rep., Riso National Laboratory, Roskilde, DK, 1983.
[5] M. Bastankhah, F. Porté-Agel, A new analytical model for wind-turbine wakes, Renew. Energy 70 (2014) 116–123.
[6] J.P. Goit, W. Munters, J. Meyers, Optimal coordinated control of power extraction in LES of a wind farm with entrance effects, Energies 9 (1) (2016) 29.
[7] J.P. Goit, J. Meyers, Optimal control of energy extraction in wind-farm boundary layers, J. Fluid Mech. 768 (2015) 5–50.
[8] R.J.A.M. Stevens, D.F. Gayme, C. Meneveau, Effects of turbine spacing on the power output of extended wind-farms, Wind Energy 19 (2) (2016) 359–370.
[9] R.J.A.M. Stevens, Dependence of optimal wind turbine spacing on wind farm length, Wind Energy 19 (4) (2016) 651–663.
[10] J.F. Herbert-Acero, O. Probst, P.-E. Réthoré, G.C. Larsen, K.K. Castillo-Villar, A review of methodological approaches for the design and optimization of wind farms, Energies 7 (2014) 6930–7016.
[11] J.F. Ainslie, Calculating the flowfield in the wake of wind turbines, J. Wind Eng. Ind. Aerodyn. 27 (1) (1988) 213–224.
[12] M.P. van der Laan, N.N. Sorensen, P.-E. Retore, J. Mann, M.C. Kelly, N. Troldborg, J.G. Schepers, E. Machefaux, An improved $k-\varepsilon$ model applied to a wind turbine wake in atmospheric turbulence, Wind Energy 18 (5) (2015) 889–907.
[13] C. Alinot, C. Masson, Aerodynamic simulations of wind turbines operating in atmospheric boundary layer with various thermal stratifications, in: ASME Wind Energy Symp., 2002, pp. 531–536.
[14] J.N. Sorensen, W. Shen, Numerical modeling of wind turbine wakes, J. Fluids Eng. 124 (2) (2002) 393–399.
[15] N. Sezer-Uzol, L.N. Long, 3-D time-accurate CFD simulations of wind turbine rotor flow fields, in: 44th AIAA Aerospace Sci., 2006, p. 394.
[16] B. Sanderse, S. Pijl, B. Koren, Review of computational fluid dynamics for wind turbine wake aerodynamics, Wind Energy 14 (7) (2011) 799–819.
[17] G.V. Iungo, V. Santhanagopalan, U. Ciri, F. Viola, Z. Lu, M.A. Rotea, S. Leonardi, Data-driven rans solver for low-computational cost simulations of wind turbine wakes, Wind Energy (2017) under review.
[18] M.A. Rotea, Dynamic programming framework for wind power maximization, in: 19th IFAC World Congress, 2013, pp. 3639–3644.
[19] E. Bitar, P. Seiler, Coordinated control of a wind turbine array for power maximization, in: American Cont. Conf. (ACC), 2013, 2013, pp. 2898–2904.
[20] G. Mosetti, C. Poloni, B. Diviacco, Optimization of wind turbine positioning in large windfarms by means of a genetic algorithm, J. Wind Eng. Ind. Aerodyn. 51 (1) (1994) 105–116.
[21] C.N. Elkinton, Offshore Wind Farm Layout Optimization, University of Massachusetts Amherst, 2007.
[22] M.I. Blanco, The economics of wind energy, Renew. Sustain. Energy Rev. 13 (6) (2009) 1372–1382.
[23] O. Arslan, Technoeconomic analysis of electricity generation from wind energy in Kutahya, Turkey, Energy 35 (1) (2010) 120–131.
[24] J. Meyers, C. Meneveau, Optimal turbine spacing in fully developed wind farm boundary layers, Wind Energy 15 (2) (2012) 305–317.
[25] R.J. Stevens, B.F. Hobbs, A. Ramos, C. Meneveau, Combining economic and fluid dynamic models to determine the optimal spacing in very large wind farms, Wind Energy 20 (3) (2017) 465–477.
[26] A. Horvat, V. Spudic, M. Baotic, Quasi-stationary optimal control for wind farm with closely spaced turbines, in: MIPRO, 35th Int. Convent. IEEE, 2012, pp. 829–834.
[27] P.M.O. Gebraad, F.C. van Dam, J.-W. van Wingerden, A model-free distributed approach for wind plant control, in: Amer. Contr. Conf., 2013, pp. 628–633.
[28] K.E. Johnson, G. Fritsch, Assessment of extremum seeking control for wind farm energy production, Wind Eng. 36 (6) (2012) 118–173.
[29] G.V. Iungo, F. Porté-Agel, Volumetric lidar scanning of wind turbine wakes under convective and neutral atmospheric stability regimes, J. Atmos. Ocean. Technol. 31 (10) (2014) 2035–2048.
[30] S. El-Asha, L. Zhan, G.V. Iungo, Quantification of power losses due to wind turbine wake interactions through SCADA, meteorological, and wind lidar data, Wind Energy (2017), http://dx.doi.org/10.1002/we.2123.
[31] M. Hall, Vortex breakdown, Annu. Rev. Fluid Mech. 4 (1) (1972) 195–218.
[32] S. Pope, Turbulent Flows, Cambridge University Press, 2000.
[33] E. Plate, Eng. Meteorol., Elsevier Sci. Pub. Co., 1982.
[34] J. Jonkman, S. Butterfield, W. Musial, G. Scott, Definition of a 5-MW Reference Wind Turbine for Offshore System Development, Tech. rep., NREL Technical Report, National Renewable Energy Laboratory, Golden, CO, 2009.
[35] Y.-T. Wu, F. Porté-Agel, Atmospheric turbulence effects on wind-turbine wakes: an LES study, Energies 5 (12) (2012) 5340–5362.
[36] M. Calaf, C. Meneveau, J. Meyers, Large eddy simulation study of fully developed wind-turbine array boundary layers, Phys. Fluids 22 (2010) 015110.
[37] M. Calaf, M.B. Parlange, C. Meneveau, Large eddy simulation study of scalar transport in fully developed wind-turbine array boundary layers, Phys. Fluids 23 (2011) 126603.
[38] F. Porté-Agel, Y.-T. Wu, H. Lu, R. Conzemius, Large-eddy simulation of atmospheric boundary layer flow through wind turbines and wind farms, J. Wind Eng. Ind. Aerodyn. 99 (4) (2011) 154–168.
[39] W. Shen, J.N. Sorensen, R. Mikkelsen, Tip loss correction for actuator/Navier-Stokes computations, in: J. Solar Energy-Trans. ASME, 127, 2005, pp. 209–213.
[40] W. Shen, R. Mikkelsen, J.N. Sorensen, C. Bak, Tip loss correction for wind turbine computations, Wind Energy 8 (2005) 457–475.
[41] R.B. Stull, An Introduction to Boundary Layer Meteorology, Kluwer Academic Publishers, 1988.
[42] J. Barradas-Berglind, R. Wisniewski, Wind farm axial-induction factor optimization for power maximization and load alleviation, in: Cont. Conf. (ECC), European, 2016, pp. 891–896.
[43] V.A. Riziotis, S.G. Voutsinas, Fatigue loads on wind turbines of different control strategies operating in complex terrain, J. Wind Eng. Ind. Aerodyn. 85 (3) (2000) 211–240.
[44] L. Hirth, The market value of variable renewables: the effect of solar wind power variability on their relative price, Energy Econ. 38 (2013) 218–236.

[45] C. Moné, A. Smith, B. Maples, M. Hand, 2013 Cost of Wind Energy, Tech. rep., National Renewable Energy Laboratory, 2015.
[46] R.E. Bellman, S.E. Dreyfus, Applied Dynamic Programming, Princeton University Press, 2015.
[47] C. Santoni, U. Ciri, M. Rotea, S. Leonardi, Development of a high fidelity cfd code for wind farm control, in: Ame. Contr. Conf. (ACC), IEEE, 2015, pp. 1715–1720.
[48] X. Liu, Z. Gao, M. Chen, Takagi-sugeno fuzzy model based fault estimation and signal compensation with application to wind turbines, IEEE Trans. Ind. Elec. 99 (2017), http://dx.doi.org/10.1109/TIE.2017.2677327.
[49] F. Shi, R. Patton, An active fault tolerant control approach to an offshore wind turbine model, Renew. Energy 75 (2015) 788–798.